

Holographic low-energy electron diffraction

This article has been downloaded from IOPscience. Please scroll down to see the full text article.

2001 J. Phys.: Condens. Matter 13 10647

(<http://iopscience.iop.org/0953-8984/13/47/308>)

View [the table of contents for this issue](#), or go to the [journal homepage](#) for more

Download details:

IP Address: 171.66.16.226

The article was downloaded on 16/05/2010 at 15:11

Please note that [terms and conditions apply](#).

Holographic low-energy electron diffraction

K Heinz¹, A Seubert¹ and D K Saldin²

¹ Lehrstuhl für Festkörperphysik, Universität Erlangen-Nürnberg, Staudtstrasse 7, D-91058 Erlangen, Germany

² Department of Physics and Laboratory for Surface Studies, University of Wisconsin-Milwaukee, PO Box 413, Milwaukee, WI 53201, USA

E-mail: kheinz@fkp.physik.uni-erlangen.de

Received 13 July 2001

Published 9 November 2001

Online at stacks.iop.org/JPhysCM/13/10647

Abstract

In holographic low-energy electron diffraction an atom protruding from a surface acts as a beam splitter for the incoming electron beam, creating a reference wave and, by subsequent substrate scattering, an object wave. In this sense, the method corresponds closely to traditional optical holography. The present power of the technique is demonstrated and sources of image degradation are pointed out. Additionally, we describe new developments designed to reduce the influence of the corresponding disturbing scattering processes. These are concerned in particular with the appearance of false atoms and incorrect atom positions. It will be demonstrated that these features can be avoided by the use of a proper kernel in the transform integral. Also, an iterative reconstruction procedure can be applied. This can also be used to reduce the influence of substrate reconstructions induced by the beam splitter, but, in that case, a hybrid of a reconstruction and a data-fitting procedure is applied.

1. Adatoms on surfaces as holographic beam splitters

It is well known that Gabor's original ideas concerning holography concentrated on electrons (to improve the resolution in electron microscopy) rather than on optical holography [1]. Yet, he was well aware of the intrinsic obstacles hindering the rapid realization of his ideas at the time. For using electrons he had to concede that ... *in light optics a coherent background can be produced in many ways, but electron optics does not possess effective beam splitting devices* ... [2]. The coherent background was meant to provide the reference wave R which is made to interfere with the wave diffracted by the object, i.e. the object wave O , in order to form the hologram. The corresponding set-up is indicated schematically on the left of figure 1, using photons rather than electrons as has become possible since the arrival of the laser. The use of a simple semi-transparent mirror as a beam splitter and the excellent coherence properties of lasers (typical order of coherence length L_c : ≈ 10 m) guarantee that R and O can interfere, as

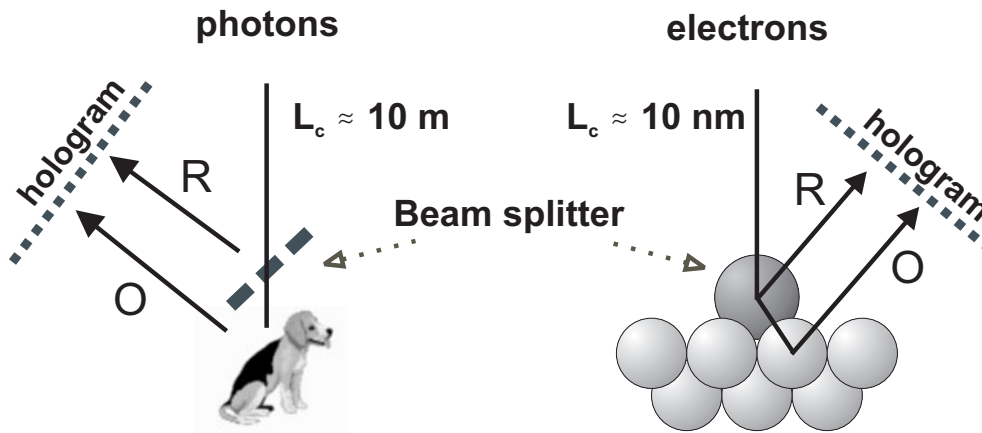


Figure 1. The principle of optical holography (left) and its analogy to LEED holography (right). The half-transparent mirror as beam splitter and the dog as object on the left are replaced by the adatom and the substrate, respectively, on the right.

the macroscopic path length between them can be held well below L_c . In contrast, L_c is of the order of only 10 nm for electron beams produced by thermal electron emitters and it was only considerably after the development of the electrostatic biprism [3] that Gabor's original ideas were found to improve the resolution of the electron microscope (see e.g. references [4–6]).

A conceptually different idea of how to realize electron holography for images providing atomic resolution was put forward by Szöke in 1986 [7]. He suggested using an atomic source of electrons within the object rather than an electron beam impinging from outside. Electrons emitted from this atom can either travel directly to the detector (reference wave) or reach it only after being scattered by atoms surrounding the emitter (object wave). Due to their path-length difference being of atomic order, i.e. smaller than L_c , the waves R and O can interfere with each other. So, the detector should record a hologram when scanning all directions of scattering. In principle, from this hologram a real-space image can be reconstructed numerically [8]. It is obvious that by use of an inner electron source both the problem of finite coherence of electron beams and the difficulties connected with effective beam-splitting devices are overcome in one step. It is also obvious, however, that due to the strong electron attenuation in solids the corresponding holographic technique is restricted to atomic images of surfaces or, more precisely, of the atomic environment of an atomic emitter within a surface. Various emitting techniques can be used and, as a consequence, different holographic techniques such as photoelectron, Auger electron and Kikuchi electron holography have emerged, as described by different authors in the present Special Issue.

The technique addressed in the present article is similar to those just mentioned, though different in detail. Like in the set-up used in low-energy electron diffraction (LEED) and as first suggested by Saldin and de Andres [9], an external electron beam impinges on the surface. In the case of a single atom adsorbed on the surface, it may hit this adatom which then acts as a beam splitter in the way indicated on the right of figure 1; i.e. a reference wave R is formed by direct back-scattering and the object wave O by forward-scattering and subsequent scattering by object atoms. Their interference pattern can be viewed as a hologram. As the beam splitter breaks the translational symmetry of the substrate, the hologram corresponds to a continuous intensity map like those known from diffuse low-energy electron diffraction (DLEED) [10–12]. When many adatoms are adsorbed in lattice-gas disorder, each of them

causes the same diffuse distribution, the sum of these contributions bringing the intensities up to a measurable level.

It is obvious from comparison of the left- and right-hand panels of figure 1 that this LEED-based holographic scenario resembles very closely that of optical holography. However, we will explain in the next section that because of the importance of dynamic, i.e. multiple-electron, scattering, things are not as simple as has been suggested up to this point (in particular as regards LEED holography) and ways to circumvent the problems will be described. Section 3 will focus on images reconstructed from continuous intensity maps and section 4 bridges to the use of conventional, i.e. discrete, superstructure beam intensities frequently caused by adsorbate layers or surface reconstruction. Special problems of image reconstructions connected with the appearance of false atoms and displaced atomic positions or beam-splitter-induced substrate reconstruction are addressed in sections 5 and 6, respectively. Conclusions and prospects for the method are presented in the last section.

2. Image reconstruction—the benefits and disadvantages of multiple scattering

It is obvious from the holographic atomic scattering processes indicated in figure 1 (right-hand panel) that multiple scattering is essential in LEED holography: whilst the lowest-order process for R is single-atomic scattering, O arises only from double scattering. So, on the one hand multiple scattering is necessary; on the other hand, however, it makes the scattering scenario rather complex as illustrated in figure 2, where we differentiate between holographic (left) and disturbing (right) processes. By the term ‘holographic processes’ we denote all processes which start at the beam splitter. The subset of these processes with the beam splitter as the last scatterer form the reference wave R_1 ; those with an atom of the substrate (=object) as the last scatterer build the object wave O_1 . In both cases there might be (additional) multiple scattering within the substrate and/or between the substrate and the beam splitter as indicated by the broken lines. The scattering processes indicated by the full lines represent the ideal holographic processes characterized by the lowest order of multiple scattering in each case.

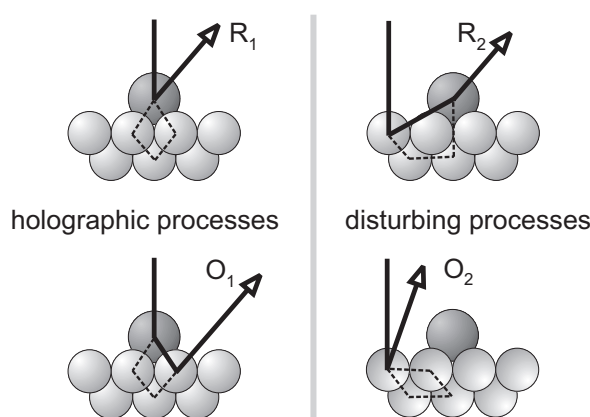


Figure 2. Holographic (left) and disturbing (right) LEED processes in an adsorbate-covered surface. In the upper panels the formation of the reference wave and in the lower panels that of the object wave is illustrated.

There are always disturbing processes for the reference wave, as represented by R_2 in the upper right panel of figure 2. Unfortunately, such processes can be of the same weight as R_1 , as in both cases only one back-scattering event is involved in the lowest order of scattering.

Generally, there is a similar contribution disturbing the object wave denoted by O_2 in the lower right panel of figure 2. However, it can only emerge in directions compatible with the substrate translational symmetry and so does not contribute to the continuous intensity distribution created by the symmetry-breaking beam-splitter atom. So, it causes no problems in many cases. Yet, there is the situation of adsorbate-induced reconstruction for which it becomes important, as we will see in section 6.

This multiple-scattering scenario in holographic LEED is unique compared to other surface holographic techniques involving e.g. photoemitted or Auger-emitted electrons. In these latter cases there is really an inner source within the surface, and *unscattered* electrons emitted from that form the reference wave, whilst those resulting from subsequent single scattering contribute to the object wave in first order. This is different from the LEED case where the first-order (holographic) object wave undergoes a double-scattering process, though if one groups together all scattering processes leaving (as the last scatterer) either the beam splitter or the substrate, there is some formal resemblance to photoelectron holography, i.e. the beam splitter plays effectively the role of an inner source. Of course, in all methods, higher orders of electron scattering also contribute to the object wave after the electron has left the beam splitter or emitter (broken-line processes in figure 2) and at first glance these processes already seem to inhibit the image reconstruction process. Even more problematic, however, is the fact that in LEED there is always the additional, non-holographic process R_2 disturbing the reference wave dramatically and there can be an additional process O_2 affecting the object wave. This means that *both* the reference and object waves are disturbed by multiple scattering, i.e. $R = R_1 + R_2$ and $O = O_1 + O_2$.

So, holographic LEED becomes possible only through multiple scattering and simultaneously seems to be inhibited by it. Fortunately, there is a way to circumvent the problem of the disturbances introduced by unwanted multiple-scattering contributions at least in the absence of adsorbate-induced reconstruction, i.e. when there are no processes of type O_2 as in the cases treated in the next two sections. The correction comes from using not just a single-energy diffraction pattern, but allowing data at many electron energies to enter the reconstruction integral. The latter contains a phase factor with the negative optical path-length difference of the ideal part of the holographic processes R_1 and O_1 given by the full-line processes on the left of figure 2. By integration over the electron energy, this acts as a stationary-phase condition which makes the transform focus on these processes and largely suppress others. This procedure, which additionally removes the twin image, was proposed first for photoelectron holography [13, 14] but appears to work for holographic LEED, too [15]. The phase mentioned is $(kr - \vec{k} \cdot \vec{r})$ where \vec{k} is the wave vector of the outgoing electron, k its modulus and \vec{r} the position of a substrate atom relative to the beam splitter which defines the origin of the coordinate system. It has been shown that, on using this stationary-phase condition, object atoms do indeed appear in the reconstructed image [16, 17]. Yet, only those object atoms which are illuminated by the forward-scattering cone of the beam splitter (the *searchlight effect*) show up; these are described by the latter's atomic scattering factor $f_b(\vec{k}_0, \vec{r})$ for scattering from direction \vec{k}_0 to \vec{r} (where \vec{k}_0 is the wave vector of the incident electron beam). With knowledge of $f_b(\vec{k}_0, \vec{r})$ —which, however, does not need to be element-specific, as most atoms have similar scattering characteristics—one can correct for the anisotropy introduced by the beam splitter using a kernel in the integral transform, $K(\vec{k}, \vec{r})$. This is given in first-order approximation by

$$K(\vec{k}, \vec{r}) \approx K_1(\vec{k}, \vec{r}) = \frac{r}{f_b(\vec{k}_0, \vec{r}) + C} \quad (1)$$

where C is an (adjustable) constant accounting additionally and in a crude way for the multiple scattering between the adatom and substrate [18]. As a result, the image reconstruction integral

is written as

$$A(\vec{r}) = \int K(\vec{k}, \vec{r}) H(\vec{k}) e^{-i(\vec{k}\vec{r} - \vec{k}\vec{r})} d^3k \quad (2)$$

where $H(\vec{k})$ represents the holographic input, i.e. the measured intensities. Of course, the back-scattering characteristics of the beam splitter and substrate atoms are both anisotropic and phase shifting. Their compensation requires an improved kernel [19]:

$$K(\vec{k}, \vec{r}) = \frac{r}{[f_b(\vec{k}_0, \vec{r}) + C] f_b^*(\vec{k}_0, \vec{k}) f_s(\vec{r}, \vec{k})}. \quad (3)$$

It has been shown recently that—when only the process R_2 is taken into account for the multiple scattering between the beam splitter and the object—the quantity C can be approximated by [19]

$$C = C(\vec{k}) = R_2^*(\vec{k}) f_b(\vec{k}_0, \vec{r}) / f_b^*(\vec{k}_0, \vec{k}). \quad (4)$$

Evidently, this contains the quantity $R_2(\vec{k})$, which depends on the (still unknown) object. It was suggested that an iterative scheme may solve this problem [19]: one might neglect C in a first step using the kernel

$$K \approx K_2(\vec{k}, \vec{r}) = \frac{r}{f_b(\vec{k}_0, \vec{r}) f_b^*(\vec{k}_0, \vec{k}) f_s(\vec{r}, \vec{k})} \quad (5)$$

and then calculate from the so-reconstructed image a first estimate of R_2 . This may then be used in equations (4) and (1), a scheme which can possibly be iterated to convergence.

3. Real-space images from diffuse intensity distributions

It is well known that adsorption of atoms on a surface, in particular at low temperatures where diffusion is inhibited, can lead to a lattice-gas-like disordered arrangement of adatoms. Each of the latter forms with its surroundings a dynamically scattering atomic cluster whose size is given by the electron attenuation length. Well below the monolayer density, i.e. when multiple scattering between different adsorbate clusters can be neglected, each of them produces the same diffuse, i.e. continuous, two-dimensional LEED intensity distribution which contains the information about the local adsorbate cluster [10, 11] (for reviews of the DLEED method, see references [12, 20]). An example is given in figure 3 for the disordered adsorption of K on Ni(100) [21].

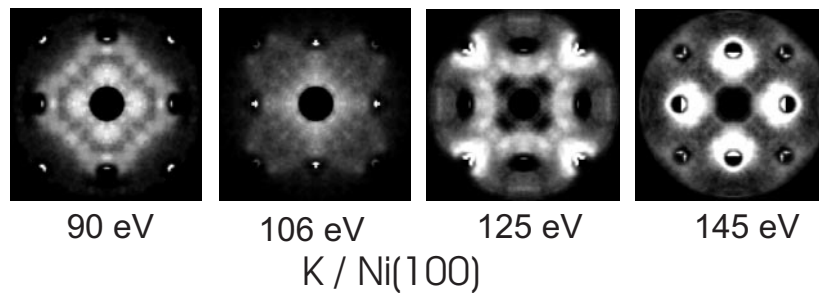


Figure 3. DLEED intensity maps for disordered K on Ni(100) measured at some selected electron energies and normal incidence of the primary beam. Bragg spots originating from substrate diffraction are cut off.

In the above-described sense these DLEED patterns can be interpreted as holograms. As expected, they vary drastically with energy as also demonstrated in figure 3. At a single energy, variation within an intensity map is with both the surface-parallel and vertical components of the wave vector, \vec{k}_{\parallel} and \vec{k}_{\perp} , respectively, so $E = \frac{1}{2}(k_{\parallel}^2 + k_{\perp}^2)$ (in atomic units) is constant. Integration in equation (2) is carried out by using $d^3k = d^2k_{\parallel} dk_{\perp}$ where an energy step width of about 5 eV (i.e. of the order of the optical potential) proves to be sufficient [15,22]. The maps were made to enter the transform integral (equation (2)) where the simplest kernel, i.e. that given by equation (1), was used according to the algorithm called ‘compensated object and reference wave reconstruction by an energy-dependent Cartesian transform’ (CORRECT) [18, 23].

Results for such image reconstructions are given in perspective in figure 4 for two cases of disordered adsorption, K/Ni(100) and O/Ni(100) [23]. The images are constructed on a real-space grid of 0.15 Å spacing and are made up of small spheres whose diameters and degrees of shading are proportional to $|A(\vec{r})|^2$ at each point. For the potassium (oxygen) adsorbate system, intensity maps in the energy range 90–152 eV (90–180 eV) were used for image reconstruction and the best image quality was retrieved for a kernel constant $C = 3.4$ Å (0.15 Å). The local adsorption geometries with nearest and next-nearest neighbours of the beam splitter clearly show up whilst the latter is, of course, not reproduced, but only defines the origin of space (it is artificially introduced into the figures for clarity). The fact that only atoms in the vicinity

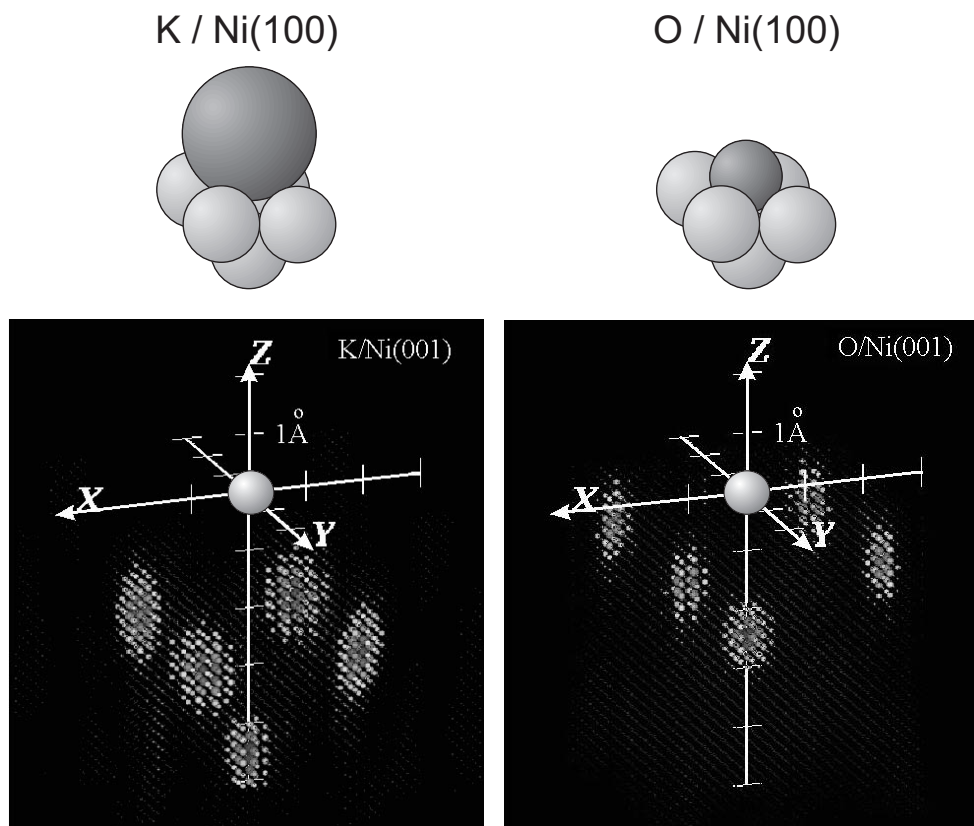


Figure 4. Real-space images reconstructed from DLEED intensity maps for disordered K/Ni(100) (left) and disordered O/Ni(100) (right) [23]. Image intensities below 40% of the maximum were interpreted as noise and are suppressed.

of the beam splitter are reconstructed is due to electron attenuation. The position of the atoms is accurate to within 0.5 \AA as judged by comparison with conventional LEED analyses of the two adsorbate systems [21, 24]. Because of its large diameter, the potassium atom resides much higher above the fourfold-symmetric hollow position than the oxygen atom, as clearly reproduced in the images.

The displacements of reconstructed atoms from their true positions are at least partly (see below) due to the non-considered scattering phase of the substrate atoms, as this simulates an additional path length (in contrast to the modulus of the scattering factor). It has been found that the anisotropy of the phase leads dominantly to lateral shifts of the object atoms, whilst its energy dependence accounts mainly for vertical displacements [25]. Corrections for that have been made by the so-called *small-cone method*, in which integration is only within a small angular cone ($\approx 25^\circ$) around the back-scattering direction defined by the connection between the object atom and beam splitter [26]. In this direction the angular variation of the scattering phase is minimal. Yet, this strategy necessarily neglects data outside the cone and so must reduce the lateral image resolution. Introducing the anisotropy and energy dependence of the scattering factor explicitly in using the appropriate integral kernel (equations (1) or (5)) circumvents this problem as will be demonstrated below. Yet, as we will also see, this does not necessarily cancel any atomic shift, as such displacements can also be induced by the contribution O_2 induced by substrate reconstruction.

In spite of the success and quality of image reconstruction achieved using DLEED intensities as demonstrated in figure 4, examples using this method are rather rare. This is certainly because of the difficulties connected with the reliable measurement of diffuse intensity distributions. Frequently they are affected by contributions of static surface defects and thermal diffuse scattering. Even if these disturbances can be subtracted, the measurement remains delicate. This is because the signal is rather weak and strong Bragg spots caused by the substrate are superimposed which blurs the signal sought, especially at higher energies when beams get crowded. Therefore, the idea of using ordered arrays of beam splitters causing discrete superstructure beams rather than diffuse intensities [27] and the eventual successful application in image reconstruction [28] allowed the use of more reliable data, and at the same time extended LEED holography to ordered superstructures. We address this in the next section.

4. Images from discrete intensity distributions

As already indicated, the measurement of discrete superstructure spot intensities—as caused by ordered adsorbates—is much easier than that of diffuse intensities. If adsorbates initially forming a disordered lattice gas subsequently form an ordered lattice, the former diffuse intensities concentrate on discrete spot positions of high local brightness, so conventional and fast measurement methods (see e.g. reference [20]) can be applied. The resulting database consists of a set of $I(E)$ spectra as used in conventional LEED analyses for surface crystallography. Yet, most of the data to be used for the holographic reconstruction seem to be lost as there are no longer intensities between the spots (though the recorded spectra undoubtedly carry all the structural information).

However, it has been shown that the grid of superstructure spots quantitatively samples the diffuse intensity distribution caused by a single adsorbate atom as long as there is no or only negligible multiple scattering between different adsorbate clusters [29, 30]. This is schematically illustrated in figure 5 where on the left the diffuse intensity distribution originating from a single adsorbate cluster is represented by broken-line arrows of different lengths (the extent of the cluster is indicated by the half-circle inserted). When the clusters

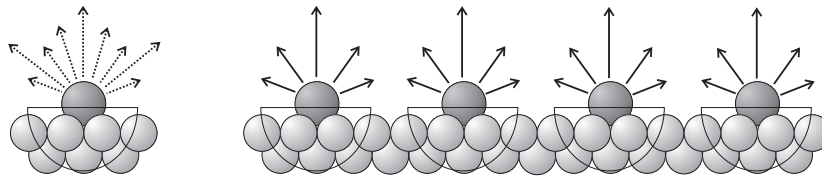


Figure 5. Formation (schematic) of diffuse intensities by a single (or many disordered) adsorbate cluster(s) (left) and of discrete superstructure beams when such clusters are ordered (right).

are ordered (right-hand panel of figure 5), only intensities in directions compatible with the translational symmetry of the adsorbate remain, as indicated by the full-line arrows. As there is no scattering between the clusters, their amplitudes just add, i.e. the intensity of the discrete beams scales with that of the former diffuse intensity in the same direction. The spatial modulation frequency of the diffuse intensities depends on the size of the atomic cluster to which multiple scattering involving the beam splitter is restricted. This is determined by electron attenuation as described by the optical potential V_{oi} . It has been shown that with a typical value of $V_{oi} \approx 4\text{--}5$ eV the grid of a (3×3) superstructure is sufficient for fully sampling the diffuse distribution [30].

Discrete spot intensities (rather than continuous contributions) can easily be made to enter the reconstruction integral, equation (2), just by replacing the integration over \vec{k}_{\parallel} by a discrete sum. This was first realized for the (3×3) superstructure of a SiC(111) surface for which STM measurements identify a single protrusion, i.e. the presence of a single beam splitter within the unit cell [28]. Here the beam splitter is a silicon atom belonging to the (3×3) reconstruction of the surface rather than being deposited in an adsorption experiment. The superstructure beam intensities were measured in the usual way up to 300 eV and used for the holographic transform, again using the simplest form of the kernel (equation (1)). This produces an excellent image quality for the reconstructed cluster [28] as displayed again in perspective in the upper left panel of figure 6 and repeated schematically on the right. In addition to the (inserted) beam splitter, the cluster consists of five clearly resolved atoms belonging to different surface layers whose spacings are indicated. The knowledge of this cluster has been decisive for the solution of the full structure both by a conventional LEED analysis [31, 32] and density functional theory (DFT) [31]. It is displayed in the lower panel of figure 6 with atoms of the reconstructed cluster shaded.

It must be mentioned that (3×3) or even larger superstructure cells with only a single surface protrusion serving as beam splitter are rather rare, and so opportunities for the application of holographic LEED in the way described may appear equally rare. Yet, it has been demonstrated [33] that the method works also for less dense sampling, using e.g. (2×2) superstructures which are observed rather frequently. As regards larger unit cells on the other hand, the chance that there is only a single beam splitter per cell decreases with increasing cell size. Yet, it has been shown that—e.g. for only two beam splitters present—the reconstructed image is a superposition of the images resulting from each adatom alone [25]. This might allow the identification of the true structure in cases that are not too complex.

5. Missing atoms, false atoms and false atom positions

It has already been mentioned that reconstructed atoms can be shifted off their true positions by of the order of 0.5 \AA and that these shifts are probably due to the (so far) non-considered phase of the scattering factor of substrate atoms. Yet, the situation can become substantially worse,

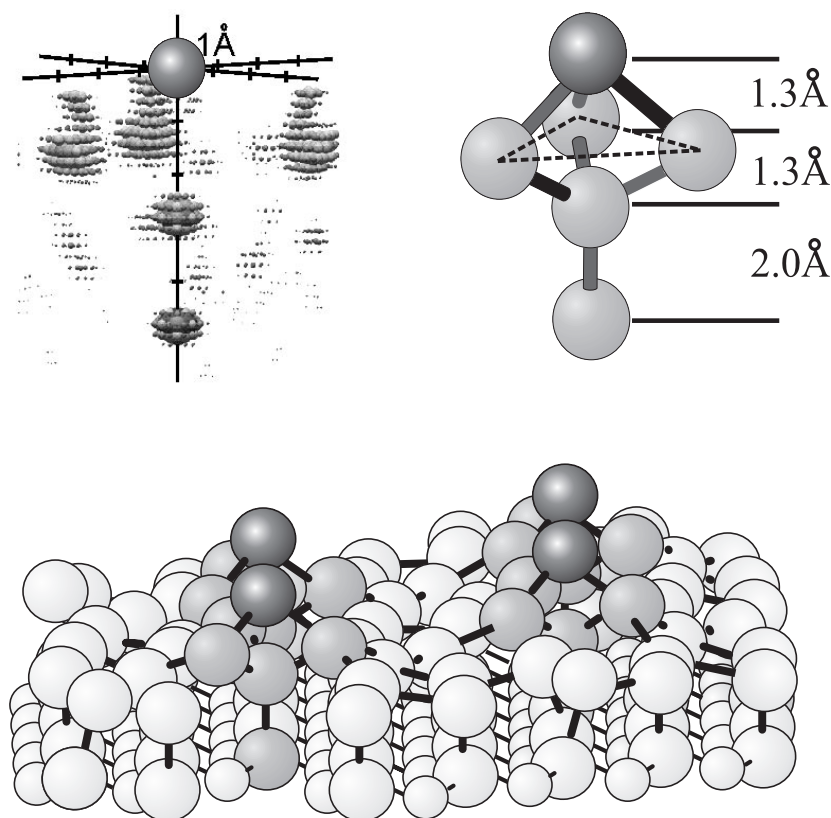


Figure 6. Reconstruction of the atomic cluster below the beam splitter (upper left, repeated schematically on the right) from discrete LEED spot intensities of SiC(111)-(3 × 3) (after reference [28]). In the lower panel the full structure is displayed, as resulting from a conventional LEED analysis [31, 32] with the cluster (heavily shaded) as input. Large spheres correspond to Si, small spheres to C atoms.

as even false atoms, i.e. ‘ghost atoms’, can appear which do not exist in the real structure. And, to make this seeming mess complete, some existing atoms or even groups of such can fail to show up at all. We recently happened to encounter a case with all of these features appearing simultaneously. This textbook case demonstrating the dangers mentioned is the $6H\text{-SiC}(0001)\text{-}(2 \times 2)_c$ phase [34, 35], where the bar in the Miller index indicates that the surface is nominally carbon terminated (the index c is present to distinguish this phase from another one of the same periodicity which is silicon rich [36]). The holographic reconstruction using the superstructure spot intensities and applying the simple transform kernel of equation (1) produces the image given on the right of figure 7 with seemingly well resolved atoms showing up. On the left the known model of the (bulk-like-terminated) substrate is displayed with possible (as yet unknown) sites of silicon adatoms indicated. Assuming that there is no drastic substrate reconstruction induced by the adsorbate, which in fact is true according to a conventional LEED analysis [34, 35], the image reconstruction should allow the identification of the adsorption site. At first glance, i.e. just by considering the arrangement of atoms and paying no attention to the absolute coordinates (as atoms can be shifted), clearly the T_4 site must be favoured. This involves identifying the atoms labelled No 1 with carbon atoms, where the appearance of a hexagon rather than a trimer is due to the superposition of two equivalent

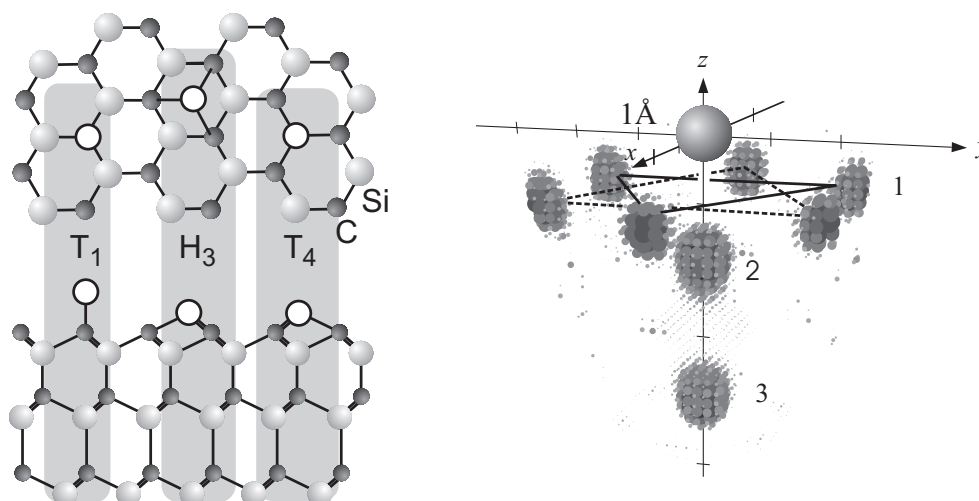


Figure 7. Image reconstruction for the $6\text{H-SiC}(000\bar{1})-(2 \times 2)_c$ phase (right panel) carried out in order to identify one of the possible adsorption sites (open circles) indicated in the surface model on the left. The model is shown in top and side view in the $[11\bar{2}0]$ direction (top and bottom, respectively). Large spheres represent Si, small ones C atoms.

surface domains, mutually rotated by 60° (only one of which is displayed in the model on the left of figure 7). Atom No 2 would then be the silicon atom in the top SiC bilayer and atom No 3 the carbon atom of the second bilayer. Yet, to cut the story short, confirmation of this T_4 site by the conventional LEED analysis already mentioned completely fails; instead the H_3 site is unambiguously resolved [34, 35].

The precise knowledge of the structure obtained through the conventional LEED allows one to identify what is wrong with the reconstructed image. This is threefold, as follows [19]:

- *Only silicon atoms show up in the image; carbon atoms are suppressed.* Consequently, atoms No 1 must be Si atoms of the top bilayer. This is only compatible with the H_3 site.
- *Atoms are considerably shifted off their true positions.* So, e.g., atoms No 1 should appear about 0.6 \AA further below.
- *Atom No 2 in the image is a ‘ghost atom’, i.e. it does not exist in the real structure.* Possibly that holds also for atom image No 3, yet this may also correspond to the (much displaced) Si atom in the third SiC bilayer or be caused by an atom in a differently terminated surface domain [34].

The easiest feature to explain is the suppression of carbon atoms. This is due to their weak scattering strength compared to that of silicon. To give an impression of the difference, figure 8 on the right compares, at the same scaling and in a scattering angle polar plot, the squared modulus of the scattering factor of silicon with that of carbon (inserted) for a typical electron energy (100 eV). As a consequence of the marked difference, the intensity spectra with and without scattering of carbon atoms considered are rather similar, as demonstrated on the left for a selected fractional-order beam of $6\text{H-SiC}(000\bar{1})-(2 \times 2)_c$. Not surprisingly therefore, the holographic image reconstruction, which uses the spectra in an integral transform, cannot resolve the carbon atoms; instead they are hidden in the image noise. It is worth noting at this point that conventional LEED—through a point-by-point comparison of the spectra—is still sensitive to the crystallographic presence of the carbon atoms [34] though, of course, the error

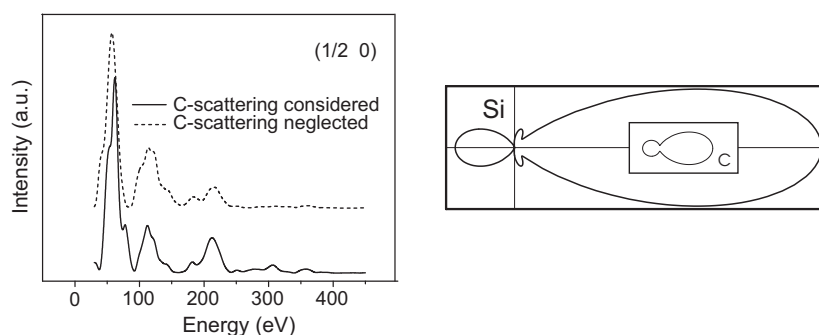


Figure 8. Comparison of intensity spectra of the $(\frac{1}{2} 0)$ spot of the phase $6\text{H-SiC}(000\bar{1})-(2 \times 2)_c$ with the scattering of carbon atoms fully considered and completely neglected (left panel). On the right the scattering factors (modulus squared) of both elements are displayed at the same scaling for an electron energy of 100 eV using a polar plot of the scattering angle.

limits concerning their positions are comparably large. This impressively demonstrates the power of full dynamical LEED structure determination.

The source of the appearance of a ghost atom is more difficult to track. Certainly, at the position of its occurrence a kind of stationary phase must exist which in turn simulates the ghost atom. It has been found that this is due to the back-scattering phases of the beam splitter and of substrate atoms not considered [19]. As has been described in section 2, this consideration is included in a first-order approximation on using the kernel given in equation (5). In fact, when one uses this kernel, the ghost atom disappears. This is demonstrated by the resulting image displayed in the right-hand panel of figure 9 and compared to a vertical cut through the real structure on the left, where atoms imaged are heavily shaded. The reader should note that again carbon atoms do not show up and that the model is only for one of two domains with only a trimer (rather than a hexamer) of silicon atoms below the beam splitter. It should also be noted that none of the silicon atoms in the second double layer of the SiC substrate shows up. This is probably due to electron attenuation which, however, should also make the image of the low-lying atom on the z -axis be similarly suppressed. Probably, the appearance of this atom is due to some forward focusing still being effective for the primary beam incident normal to the surface. We also mention that the transform in equation (2) on the z -axis (i.e. for $x = y = 0$) is equivalent to the Patterson transform [37] which—in the case of single scattering—reproduces interatomic vectors, so the signal might be stronger at the related positions.

Figure 9 shows that the atoms below the beam splitter are still displaced from the real positions, in spite of using a kernel which corrects (in kinematic approximation) for the phases of the atomic form factors. Also, the reconstructed image is considerably affected by noise. Tests using calculated rather than measured spectra and considering all processes $O = O_1$ and $R = R_1 + R_2$ yield images with much less noise and the atoms at their correct positions. So, there must be an additional disturbance. This comes through the process O_2 mentioned already in section 2 and this brings us to the next section.

6. Beam-splitter-induced subject reconstruction: problem and solution

Up to this point it was assumed that contributions to diffuse intensity distributions (section 3) or to discrete superstructure spot intensities (section 4) arise only from scattering processes involving the beam-splitter atom. Yet, when the latter induces a reconstruction of the substrate

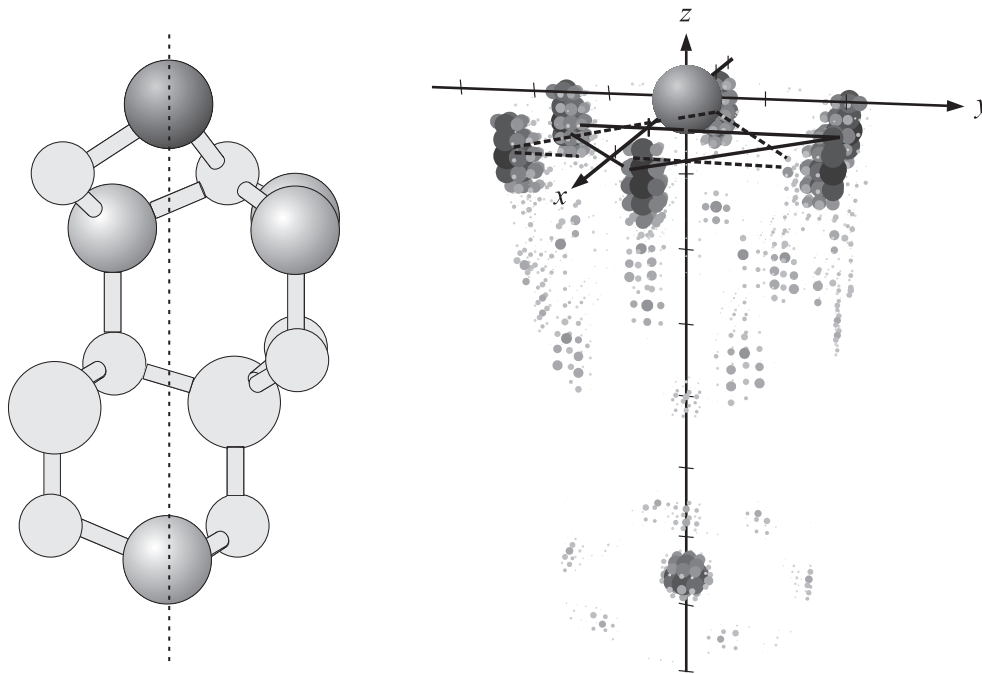


Figure 9. Image reconstruction (right) for $6\text{H-SiC}(000\bar{1})-(2 \times 2)_c$ using the kernel of equation (5) which accounts for the phases of all scattering factors involved. On the left a vertical cut through the real structural model is given (for one domain only) with the atoms reproduced in the image heavily shaded. Large spheres denote silicon, small ones carbon atoms.

this is no longer true and there are contributions from substrate scattering with the beam splitter never encountered. This was indicated by the process labelled O_2 in figure 2. This process, which can be generalized to include also multiple scattering within the substrate, appears to be the most difficult to handle as it is not a holographic process at all (in the sense described) but only disturbs the hologram. Of course, if the reconstruction is weak enough there is no problem, as is the case for e.g. $\text{O/Ni}(100)$ which exhibits only some small substrate reconstruction [24] and so still allows a reliable image reconstruction as shown above.

Indeed, the situation in the case of $6\text{H-SiC}(000\bar{1})-(2 \times 2)_c$ is different in this respect. In the (2×2) unit cell there are silicon atoms in the first double layer of the SiC substrate that are differently coordinated with respect to the adatom in the H_3 position (as indicated by atoms labelled 1 and 2 in figure 10). The conventional LEED analysis [34, 35] shows that this leads to a buckling of amplitude $b = -0.2 \text{ \AA}$ in this silicon layer, where the minus sign indicates that the atoms of type 1 are pushed into the surface relative to atoms of type 2. Though the buckling is not dramatic, it induces a strong contribution O_2 which adds to the total object wave ($O = O_1 + O_2$). To allow estimation of the importance of O_2 , the spectrum of its modulus squared is displayed in the right-hand panel of figure 10. Evidently it is much larger than the intensities corresponding to the ideal holographic processes O_1 and the disturbance of the reference wave R_2 which are shown on the same scale for comparison. The discrepancy is so large that one feels surprised that the holographic reconstruction produces any atomic-like images. Obviously, even in this rather unfavourable case the image suffers only from displaced atoms (and from some noise)—see figure 9—with the general features of the cluster still recovered. This is very much analogous to the manner in which a known form of signal

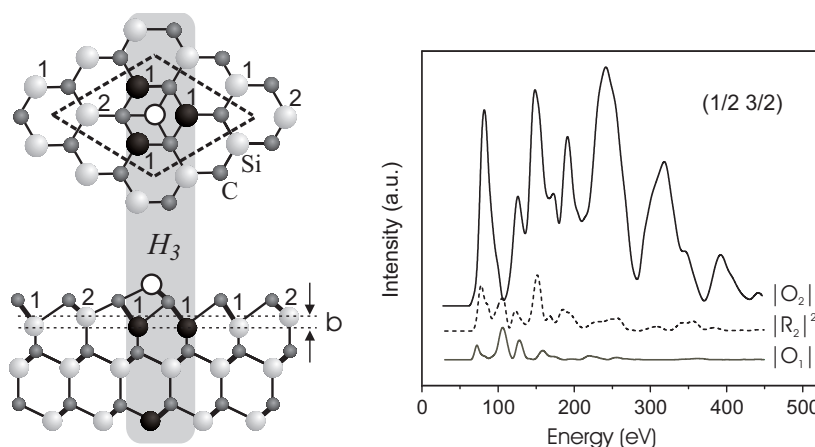


Figure 10. A model of the $6H\text{-SiC}(000\bar{1})\text{-}(2 \times 2)_c$ phase in top and side view (left) with the (2×2) unit cell indicated. On the right, the process O_2 induced by the substrate buckling is compared to processes R_2 and O_1 (see figure 2), in the form of the modulus squared in each case.

(in the present case an *elementary hologram* [38] from a single atom) may be extracted from below the level of the ambient noise, as in the technique of matched filtering [39].

Nevertheless, it seems clear that the atomic shifts mentioned and visualized in figure 9 can only be removed by removing the disturbing signal O_2 . However, we lack knowledge of this signal in the first place, as it is caused by the very object structure that we are seeking. Yet, as only atoms surrounding the beam splitter are imaged (here type 1), one can or even must always imagine that other atoms in the unit cell and in the same layer (here atoms of type 2) may be located at positions inequivalent to those of the imaged atoms, so a contribution O_2 is created. One can then calculate intensity spectra under variation of these positions (but keeping the location of the other atoms fixed as imaged). From the fit to the experimental data a first guess for the position of the non-imaged atoms results, i.e. in the present case for the buckling b . With this information one can—in a first-order approximation—calculate O_2 and all the terms in the total intensity $I = |R + O|^2$ affected by it and subtract them from the experimental data. The so-corrected data set is then made to enter the holographic transform again and a—one hopes improved—new image is reconstructed. The procedure described can be iterated until (again, one hopes) convergence is achieved. Of course, in taking this approach the strictly direct road of image reconstruction is left. Instead, it represents a kind of hybrid, i.e. a combination of data fitting and holographic data evaluation.

The performance of this procedure for the above case of $6H\text{-SiC}(000\bar{1})\text{-}(2 \times 2)_c$ is illustrated succinctly in figure 11 (more details of the method can be found in reference [41]). We take advantage of the fact that we know the real structure and so the real contribution O_2 , so we can compare it to the approximations achieved in each iterative step. In order to avoid complications caused by the superposition of different mutually rotated domains, we replaced the experimental intensities by data calculated for a single domain. They are called pseudo-experimental data in the following. The atomic image reconstructed from these intensities is displayed in the lower left panel of figure 11 as our zero approximation (in view of the single-domain intensities used, the image is now of threefold rotational symmetry). Of course, there is no information about the location of atoms which are missing in the image (silicon atom No 2) because they are too distant from the beam splitter. This comes in the first step of the iteration in which the positions of the atoms resulting from the zero-order

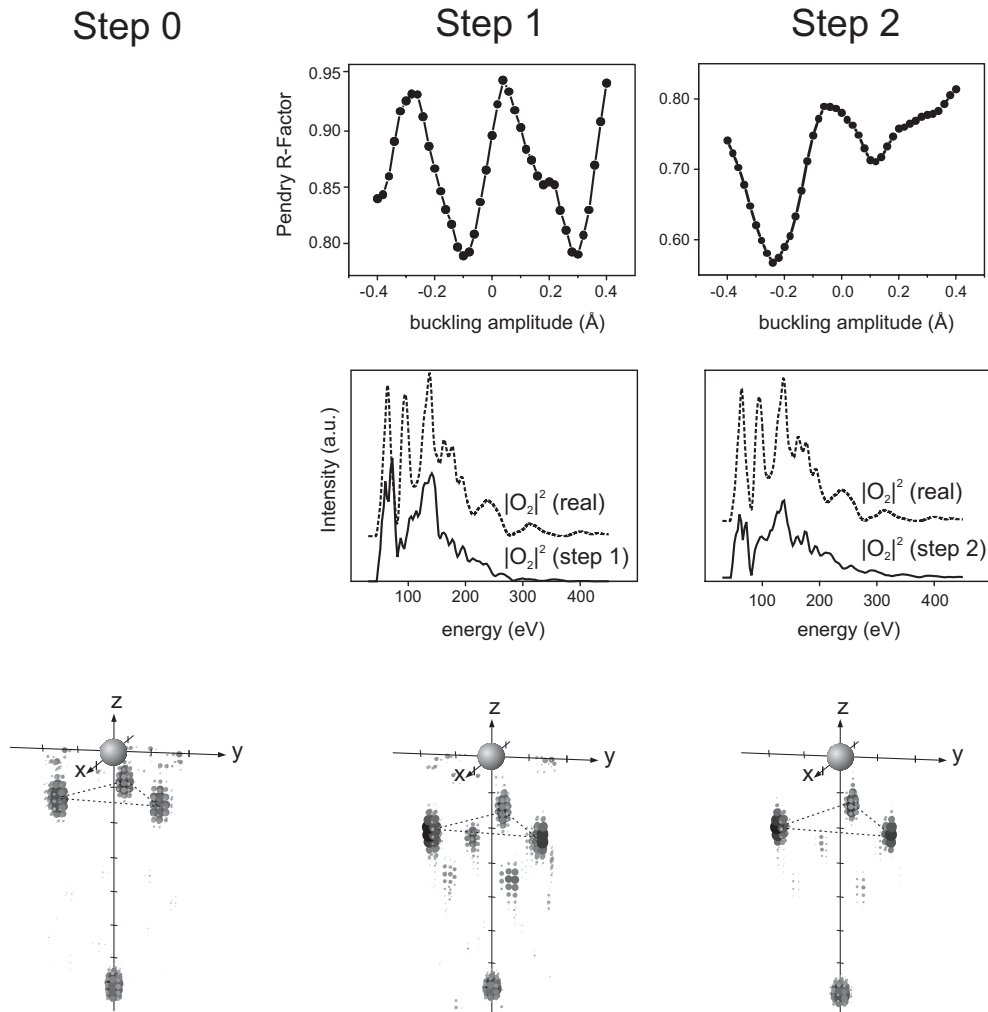


Figure 11. The performance of the iterative image reconstruction procedure for $6\text{H-SiC}(000\bar{1})-(2 \times 2)_c$ in order to reduce disturbances caused by adsorbate-induced substrate reconstruction. For details, see the text.

image are kept fixed and the vertical coordinate of silicon atom No 2 is varied. The fit to the pseudo-experimental intensities according to this variation is displayed in the top middle panel of figure 11 as quantified by the Pendry R -factor [40]. There are two minima of almost the same depth leading to two different bucklings of the silicon layer. Of course, the two minima must be considered as different structural cases for the calculation of the wave O_2 . We proceed here by choosing the second minimum, as it has the wrong sign and so might present a kind of worst case (however, we emphasize that taking the other minimum eventually leads to the same result in the final iterative step [41]). The quantity $|O_2|^2$ computed from the corresponding structure is compared to its real spectrum in the middle panel of the middle row in figure 11 at the same scaling (only shifted for clarity). Evidently, it is already of the correct order of magnitude, and many spectral features show up correctly, also. The initial pseudo-experimental data set is now corrected for all interference terms with O_2 involved

and a new image reconstruction is executed with the corrected data. Its result is displayed in the lower middle panel of figure 11. Apparently, the formerly displaced atoms have already shifted to almost exact positions, though the image suffers from some increased noise. This noise disappears if one repeats the procedure described to one further step as demonstrated in the right-hand panels of figure 11. Now there is only a single minimum in the R -factor curve which practically hits the correct value ($b = -0.2 \text{ \AA}$). The quantity $|O_2|^2$ is even closer to the real spectrum, though it is far from coincident. This is due to the fact that also the layer of carbon atoms is buckled which, however, obviously does not degrade the image quality.

As pointed out, the success of the iteration procedure does not depend on the R -factor minimum chosen in the first step [41]. We also note, however, that using real experimental intensities (instead of pseudo-experimental data as above) is not unproblematic. This is because the level of experimental intensities is always considerably below that of computed ones, a circumstance due to surface defects or completely disordered patches on the surface. As a consequence, the amount by which the calculated intensities must be reduced to fit to the experiment is *a priori* unknown. This is unimportant for the theory–experiment fit in conventional LEED analyses when an R -factor relying on derivatives (e.g. the Pendry R -factor [40]) rather than using absolute intensities is applied. Yet, even in the latter case one can normalize the two levels to each other. However, this may not work in the iterative scheme presented above as we have to correct for only a part of the scattering processes whose real, i.e. experimental, weight is not known. We are currently working on this problem.

7. Conclusions and prospects

As demonstrated in the above sections, the holographic reconstruction of atomic real-space images directly from measured intensity spectra, $I(E)$, is possible and unproblematic

- when there is a single surface-protruding atom per unit cell serving as a well defined beam splitter *and*
- when there are no or only negligible intensity contributions to superstructure spots (or diffuse intensities) from processes not having encountered the beam splitter.

In cases meeting these conditions, atomically well resolved images result immediately. The atoms appear at their correct positions when a proper integral kernel is used in the transform. This must correct for the energy-dependent and anisotropic scattering of *all* atoms involved with respect to both the modulus and phase of the atomic scattering factor. The corrections enforce the working of the stationary-phase condition used in the transform integral which suppresses non-holographic scattering processes. This holds largely also for the process R_2 which disturbs the reference wave by the (unknown) substrate scattering, at least in the examples treated in the literature up to now. We note that the beam splitter need not necessarily be deposited on the surface by adsorption, but may be part of the surface structure, as was the case for the reconstructed silicon carbide surfaces in the examples above. The reader should also be aware of the fact that the atomic positions are not resolved with the same accuracy as in conventional LEED, which quite frequently approaches the order of 0.01 \AA . Therefore, each holographic image reconstruction should be followed by a refinement by means of conventional LEED which, as the structural model and the approximate atomic coordinates are retrieved by the image, is easy to do.

When one of the above two conditions is not met, holographic LEED has a problem. For the second case, i.e. the disturbance of the object wave by substrate reconstruction (process O_2), we were able to offer a way out in the present paper. This is by the use of an iterative scheme to calculate the disturbing contributions and using them for the correction of the

intensities entering the holographic transform (we note that an iteration scheme can also be used to calculate the contribution R_2 which disturbs the reference wave [19]). In the case presented, the signal coming from the substrate reconstruction is very strong, equivalent to a strong disturbance of the object wave. As even in this rather unfavourable case, only two steps of iteration are needed, we are confident that the method will work for a rather large class of structures. Yet, it is important to point out that the method proposed is no longer fully direct, as some fitting of calculated to measured data is involved. However, as only the positions of atoms missing in the image are varied in the fit, the method compromises between the conventional full structural search and the fully direct (i.e. holographic) data evaluation and it is clearly a hybrid in this sense.

Though it is unlikely that small superstructure cells contain more than one beam splitter, this may happen with larger cells and then the other of the above conditions fails to be met. This situation is more serious as there is no well defined reference wave at all. As already mentioned in section 4, in favourable cases the total image is a superposition of the images that each of the beam splitters would create on their own. Yet, even that can lead to confusing situations when, say, more than two beam splitters are involved. In such cases one might use the trick of depositing additional atoms on the surface, which, however, should not disturb the structure to be investigated. So, one might use a rare-gas atom, e.g. xenon, which would have the additional advantage of being a strong scatterer and so a rather effective beam splitter. Another way out would be to take the scattering contribution of a whole part of a structure, which is known *a priori* (e.g. from scanning tunnelling microscopy), as the reference wave and to holographically reconstruct the rest of the structure, possibly in an iterative way. Summarizing, it appears that holographic LEED in its present state can already be applied successfully for many structural cases with surface unit cells that are not too large. Also, there is a great potential for the method to be developed to apply also to more complex cases in the future.

Acknowledgments

This work was supported by the Deutsche Forschungsgemeinschaft (DFG) through Sonderforschungsbereich 292, and by the US National Science Foundation (NSF), through grant number DMR-9815092.

References

- [1] Gabor D 1948 *Nature* **161** 777
- [2] Gabor D 1949 *Proc. R. Soc. A* **197** 454
- [3] Möllenstedt G and Dücker H 1955 *Naturwissenschaften* **42** 41
- [4] Tonomura A 1994 *Electron Holography* (Berlin: Springer)
- [5] Orchowski A, Rau W D and Lichte H 1995 *Phys. Rev. Lett.* **74** 399
- [6] Lichte H 1997 *Electron Holography Methods (Handbook of Microscopy Methods vol 1)* ed S Amelinckx, D van Dyck, J van Lunduyt and G van Tendeloo (Weinheim: VCH) p 515
- [7] Szöke A 1986 *Short Wavelength Coherent Radiation: Generation and Applications (AIP Conf. Proc. No 147)* ed D J Atwood and J Boker (New York: American Institute of Physics)
- [8] Barton J J 1988 *Phys. Rev. Lett.* **61** 1356
- [9] Saldin D K and de Andres P L 1990 *Phys. Rev. Lett.* **64** 1270
- [10] Pendry J B and Saldin D K 1984 *Surf. Sci.* **145** 33
- [11] Heinz K, Saldin D K and Pendry J B 1985 *Phys. Rev. Lett.* **55** 2312
- [12] Starke U, Heinz K and Pendry J B 1996 *Prog. Surf. Sci.* **52** 53
- [13] Tong S Y, Hua Li and Huang H 1991 *Phys. Rev. Lett.* **67** 3102
- [14] Barton J J 1991 *Phys. Rev. Lett.* **67** 3106
- [15] Wei C M and Tong S Y 1992 *Surf. Sci.* **274** L577

- [16] Wei C M, Tong S Y, Wedler H, Mendez M A and Heinz K 1994 *Phys. Rev. Lett.* **72** 2434
- [17] Heinz K and Wedler H 1994 *Surf. Rev. Lett.* **1** 319
- [18] Saldin D K and Chen X 1995 *Phys. Rev. B* **52** 2941
- [19] Seubert A, Saldin D K, Bernhardt J, Starke U and Heinz K 2000 *J. Phys.: Condens. Matter* **12** 5527
- [20] Heinz K 1995 *Rep. Prog. Phys.* **58** 637
- [21] Wedler H, Mendez M A, Bayer P, Löffler U, Heinz K, Fritzsche V and Pendry J B 1993 *Surf. Sci.* **293** 47
- [22] Heinz K, Starke U and Bernhardt J 2000 *Prog. Surf. Sci.* **64** 163
- [23] Saldin D K, Chen X, Vamvakas J A, Ott M, Wedler H, Reuter K, Heinz K and de Andres P L 1997 *Surf. Rev. Lett.* **4** 991
- [24] Oed W, Lindner H, Starke U, Heinz K, Müller K, Saldin D K, de Andres P L and Pendry J B 1990 *Surf. Sci.* **225** 242
- [25] Wedler H 1997 *PhD Thesis* University of Erlangen-Nürnberg
- [26] Tong S Y, Hua Li and Huang H 1994 *Surf. Rev. Lett.* **1** 303
- [27] Mendez M A, Glück C and Heinz K 1992 *J. Phys.: Condens. Matter* **4** 999
- [28] Reuter K, Bernhardt J, Wedler H, Schardt J, Starke U and Heinz K 1997 *Phys. Rev. Lett.* **79** 4818
- [29] Heinz K, Starke U and Bothe F 1991 *Surf. Sci.* **243** L70
- [30] Heinz K, Starke U, Van Hove M A and Somorjai G A 1992 *Surf. Sci.* **261** 57
- [31] Starke U, Schardt J, Bernhardt J, Franke M, Reuter K, Wedler H, Heinz K, Furthmüller J, Käckel P and Bechstedt F 1998 *Phys. Rev. Lett.* **80** 758
- [32] Schardt J, Bernhardt J, Starke U and Heinz K 2000 *Phys. Rev. B* **62** 10 335
- [33] Reuter K, Vamvakas J A, Saldin D K, Blum V, Ott M, Wedler H, Döll R and Heinz K 1998 *Phys. Rev. B* **58** 4102
- [34] Seubert A, Bernhardt J, Nerding M, Starke U and Heinz K 2000 *Surf. Sci.* **454–456** 45
- [35] Bernhardt J, Seubert A, Nerding M, Starke U and Heinz K 2000 *Mater. Sci. Eng. B* **338–342** 345
- [36] Bernhardt J, Nerding M, Starke U and Heinz K 1999 *Mater. Sci. Eng. B* **61+62** 207
- [37] Chang C Y, Liu Z C, Chou Y C and Wei C M 1999 *Phys. Rev. Lett.* **83** 2580
- [38] Szöke A 1993 *Phys. Rev. B* **47** 14 044
- [39] Wainstein L A and Zubakov V D 1962 *Extraction of Signals from Noise* (London: Prentice-Hall)
- [40] Pendry J B 1980 *J. Phys. C: Solid State Phys.* **13** 937
- [41] Seubert A and Heinz K 2001 in preparation